



## ORIGINAL ARTICLE

# The effect of using albumin-perfluorohexane/cisplatin-magnetite nanoparticles produced by hydrothermal method against gastric cancer cells through combination therapy



Dongsheng Li<sup>a,1</sup>, Yue Fan<sup>b,c,1</sup>, Miaomiao Liu<sup>a</sup>, SiLin Huang<sup>d,e,f,\*,1</sup>, Shasha Wang<sup>g</sup>

<sup>a</sup> Department of General Surgery, The First Affiliated Hospital of Jinzhou Medical University, Jinzhou 121000, China

<sup>b</sup> Discipline Construction Office, Southern University of Science and Technology Hospital, Shenzhen 518071, China

<sup>c</sup> Information Resource Center, Institute of Scientific and Technical Information of China, Beijing 100105, China

<sup>d</sup> Department of Gastroenterology, South China Hospital, Medical School, Shenzhen University, Shenzhen 518116, China

<sup>e</sup> Faculty of Life Science and Technology, Kunming University of Science and Technology, Kunming 650500, China

<sup>f</sup> Medical School, Kunming University of Science and Technology, Kunming 650500, China

<sup>g</sup> Department of Oncology, Qingdao Municipal Hospital, Qingdao 266000, China

Received 25 June 2021; accepted 27 February 2023

Available online 4 March 2023

## KEYWORDS

Gastric cancer;  
Photothermal therapy;  
Chemotherapy;  
Magnetic nanoparticle;  
Cisplatin

**Abstract** Because magnetic nanoparticles (NPs) have the ability to combine different therapies such as drug delivery and photothermal therapy (PTT) along with reducing cancer drug resistance, their use in cancer treatment is considerable. For this purpose, we developed albumin-perfluorohexane/cisplatin-magnetite NPs (A-PFH/C-MNPs) by hydrothermal method. Then, the physicochemical properties of the MNPs and A-PFH/C-MNPs were investigated by SEM, TEM, XRD, and FTIR. In the following, drug release at different pH and A-PFH/C-MNPs thermal reactions were assessed. The toxicity of different drug formulations against advanced gastric cancer (AGS) and mouse fibroblast (3 T3) cells were assessed by MTT assay, followed by flow cytometry and real time PCR on AGS cells. The results determined that A-PFH/C-MNPs (~142 nm) with a relatively uniform distribution, in addition to increasing the loading capacity up to 60%, raise the PFH release by increasing the temperature from 37 °C to 45 °C. Also, *in vitro* outcomes exhibited higher toxicity

\* Corresponding author at: No. 1, Fuxin Road, Longgang District, Shenzhen, Guangdong Province, China.

E-mail address: [silinhuang@szu.edu.cn](mailto:silinhuang@szu.edu.cn) (S. Huang).

<sup>1</sup> Contributed equally to this study.

Peer review under responsibility of King Saud University.



of A-PFH/C-MNPs + PTT compared to free C against AGS cells. Whereas, the toxicity of A-C-MNPs and A-PFH/C-MNPs + PTT on 3 T3 cells as normal cells was much lower compared to the cancer cells. The mechanism of cytotoxicity indicates that A-PFH/C-MNPs + PTT significantly increase apoptosis by inducing expression of TNF- $\alpha$  and Bax mRNA compared to A-C-MNPs. Overall, A-PFH/C-MNPs + PTT provided a promising platform in anticancer activity by increasing drug loading capacity and combined chemotherapy and PTT.

© 2023 Published by Elsevier B.V. on behalf of King Saud University. This is an open access article under the CC BY-NC-ND license (<http://creativecommons.org/licenses/by-nc-nd/4.0/>).

## 1. Introduction

Gastric cancer is one of the most deadly and malignant cancers in the world with a high prevalence and mortality rate (Thrift and El-Serag 2020). Despite significant advances in the diagnosis of gastric cancer in its early stages (Shimura et al. 2020), it is considered as a challenging issue due to drug resistance with high mortality rates (Marin et al. 2020). Although several conventional treatments for cancer, such as radiotherapy, chemotherapy, and surgery have been developed, researchers are developing nanotechnology-based hybrid methods to reduce the side effects of treatment, reduce the dose of the drug, and deliver drugs more effectively (Liang et al. 2020, Xiao et al. 2020). Therefore, in order to reduce the toxicity of drugs used through targeting, increasing drug loading in cancer cells, induction of cell death pathways along with enhancing auxiliary therapeutics, the use of biocompatible nanoparticles (NPs) with high loading, and the possibility of performing therapeutics such as photo or thermal therapy were widely considered (Khan et al. 2021).

Among the metal NPs used in the treatment of cancers, the use of magnetite NPs (MNPs) due to very low toxicity, cheap production, simple drug loading, the ability to perform various therapeutics and low immunogenicity are also considered by researchers (Bejjanki et al. 2021). Also, the use of MNPs is a good option for therapeutics due to its high ability to generate heat by absorbing light wavelengths in a range that has no effect on the biological system (Batooei et al. 2020, Nagaraju et al. 2021). In fact, heat absorption from light absorbs apoptosis by increasing the intracellular reactive oxygen species (ROS) (Agnihotri et al. 2020). For example, in the cellular model, Norouzi et al. (2020) were able to not only amplify the inhibition of glioblastoma cancer cells by targeting them with trimethoxysilylpropyl-ethylene nediamine triacetic acid-coated MNPs containing doxorubicin, but also to provide more effective control through synergy with magnet therapy. Likewise, Sharifi et al. (2020a), and Maximenko et al. (2020) revealed that MNPs containing anticancer drug, in addition to reducing cancerous cell proliferation through combination with photothermal therapy (PTT), enable more effective control of cancer cells with minimal toxicity and immunogenicity. In this regard, Chen and Yang (2020) provided a higher contrast of gastric cancer cells in imaging by using glypican-3 protein on MNPs.

Cisplatin (C) is a chemical compound with a high degree of toxicity that is widely used in the treatment of various cancers with a toxicity rate of more than 60% (Yu et al. 2020). It was formerly known as Peyronie's chloride and was first synthesized in 1845 by Michele Peyrone (Prestayko 2013). The most important mechanisms described in the treatment of gastric cancer by cisplatin have anti-neoplastic effects including induction of apoptosis through DNA damage (Chen et al. 2018), ROS production (Lin et al. 2019), cell cycles arrest in the subG1 phase (Song et al. 2016), and disruption of mitochondrial activity (Chen et al. 2017). However, reports indicate that cancer cells show cisplatin resistance after drug therapy (Manohar and Leung 2018, Ghosh 2019). However, hypoxia in tumors challenges the possibility of drug delivery. For this purpose, various strategies to reduce hypoxia, such as the use of O<sub>2</sub> transport by PFH (Xu et al. 2016) and in-situ O<sub>2</sub> production by nanozymes (Jiang et al. 2019), have been investigated. PFH have been widely commercialized as O<sub>2</sub> carriers to overcome hypoxic conditions due to their high affinity for O<sub>2</sub> and good biocompatibility

along with a boiling point of 56 °C and stability in tissues (Yu et al. 2018, Wang et al. 2020). Meanwhile, due to the property of phase transition caused by temperature, PFH have been investigated as contrast agents (Wang et al. 2020). The synergy of PDT with PFH not only increases the O<sub>2</sub> level, but also increases the lifetime of ROS within the tumor due to its ROS storage capability (Zhou et al. 2016, Wang et al. 2020).

In this study, with the production of albumin-perfluorohexane/cis platin-MNPs (A-PFH/C-MNPs), in addition to reducing the drug resistance of gastric cancer, the combination of PTT with chemotherapy was investigated. Also, in addition to explaining the toxicity of A-PFH/C-MNPs, an attempt was made to investigate the C and PFH release profile *in vitro*. Also, in this study, the toxicity mechanism of A-PFH/C-MNPs in gastric cancer cells was evaluated (Fig. 1A). In fact, our goal was to provide a biocompatible platform for combining therapeutics with a minimally invasive approach to reduce the therapeutic resistance of gastric cancer cells and their effective treatment.

## 2. Experimental section

### 2.1. Synthesis of A-PFH/C-MNPs

MNPs were designed by the hydrothermal method via a ligand-assisted method described by Su et al. (2015). In summary, initially 2 mL of oleic acid was dissolved in 20 mL of ethylene glycol. Then 20 mM of ferric chloride hexahydrate FCH and 40 mM of sodium acetate were added to the solution. Then, the mixture was stirred for 24 h at 60 °C. Finally, it was heated in a Teflon-lined stainless-steel autoclave at 220 °C for 8 h. After cooling at room temperature, the MNPs were collected by centrifugation (at 7,000 rpm for 12 min) and washed with ethanol and water.

The method described by Sharifi et al. (2020c) was used for more stable loading of A and other compounds on MNP. In brief, to provide hydroxyl functional groups on the surface of PFH/C-MNPs, 1 mg/mL of NPs with 40  $\mu$ L of N-hydroxysuccinimide (0.1%) and 40  $\mu$ L of 1-Ethyl-3-(3-dimethylaminopropyl) carbodiimide for 3 h at 4 °C were vigorously stirred. Then, after using the PD-10 column moderated with 10 mM PBS solution, dissolved the MNPs in DI water and mixed 2 mg of A (500  $\mu$ L) and stirred at 21 °C for 24 h. Finally, the resulting product was rinsed with water for later use.

Based on the optimum point obtained in the MNPs loading capacity, we mixed 1 mg of MNPs with 2 mL of DMSO solution containing 2 mg of C and stirred for 24 h. The solution was then dried under vacuum to evaporate the excess DMSO within 24 h. Using the phosphate buffer saline (PBS), removed the excess C by washing 3 times. To load the PFH onto the MNPs containing the C, the C-MNPs were kept in a sealed container for 2 h at 21 °C after mixing with the PFH and sonication. To remove excess agents, the mixture was first

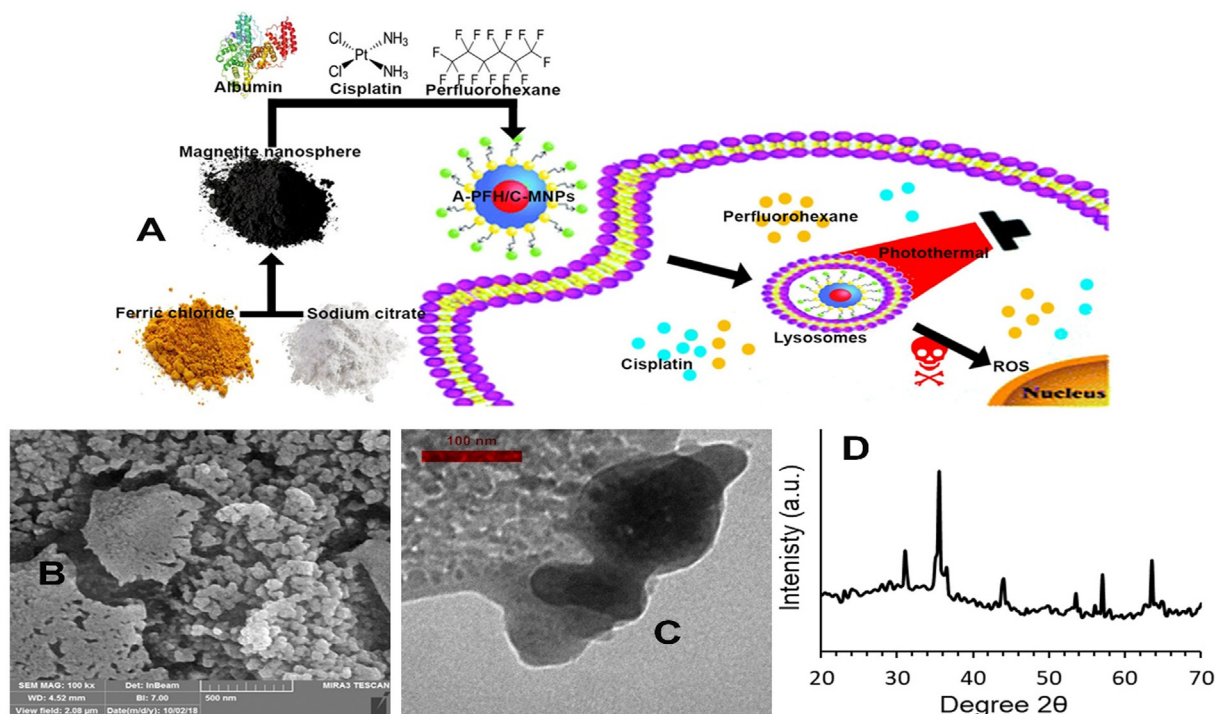


**Fig. 1** (A) Scheme of the perfluorohexane and cisplatin release by A-PFH/C-MNPs. (B) FE-SEM and (C) TEM images of A-PFH/C-MNPs. (D) XRD patterns of MNPs.

centrifuged at 5000 rpm for 10 min and then washed with deionized (DI) water.

### 2.2. Characterization of A-PFH/C-MNPs

To evaluate the appearance of A-PFH/C-MNPs, scanning electron microscopy (SEM, JEOL, JSM 6701F) was applied, and high-resolution images were obtained by using a transmission electron microscope (TEM-JEOL3010). The crystal microstructure of the produced MNPs was investigated using Power X-ray Diffractometer (Phillips, USA). The measurements were carried out in the standard 2θ applying Cu Kα radiation ( $\lambda = 0.154$  nm). The data were gathered in the range between 20° to 70° with a step size of 0.08°. In the following, further features of the A-PFH/C-MNPs was carried out using a Perkin Elmer spectrometer FTIR SPECTRUM in wavenumbers from 4000 to 500  $\text{cm}^{-1}$  by a KBr wafer. To determine the rate of temperature, increase in A-PFH/C-MNPs by PTT, a thermometer was used during the radiation with a wavelength of 808 nm.

### 2.3. C loading and C or PFH release

In order to evaluate the drug loading capacity of MNPs, the fluorescence spectra method was used by Hitachi F 2500 spectrophotometer. In this method, 0.6 mg of MNPs are added to the solutions with concentrations of 50, 150, 300, 450, 600  $\mu\text{g}/\text{mL}$  of the C and stirred for 24 h at 21 °C. The C-MNPs were then separated from the solution using a magnet and the percentage of drug charge was determined.

After determining the optimum point by loading efficiency (%), we dissolved 2 mg of MNPs with 1 mg of C in 2 mL of DMSO and shaken for 24 h at 21 °C. Then, according to the

above method, the MNPs containing the C were loaded with PFH and coated with A. Finally, the A-PFH/C-MNPs are dried in vacuum and washed 3 times with water. Then, to evaluate the release of the C through dialysis bags, certain amounts of A-PFH/C-MNPs are incubated in 20 mL of PBS at different pHs (2.5, 5.0 and 7.5) at 37 °C for 1800 min. Next, purification was performed by a dialysis process (MWCO 3500) against 80 mL of the same buffer at 100 rpm. At regular time intervals, 10 mL of solution was drawn for the measurement by absorbance at 510 nm. At the time of extraction from the solution an equal volume of the same solution was recovered.

In order to evaluate the loaded amount of PFH, A-PFH/C-MNPs were first weighed. The A-PFH/C-MNPs were then placed at 37, 41 and 45 °C to evaporate the PFH. The NPs were then weighed again after 60 min. The amount of PFH loaded was calculated using the weight loss caused by PFH evaporation.

### 2.4. Cell culture

The human gastric carcinoma cell line (AGS) and the mouse fibroblast cell line (3 T3) were obtained from American Tissue and Culture Collection (ATCC) (Manassas, VA, USA). The 3 T3 and AGE cells were cultured in DMEM and RPMI-1640 medium, respectively containing 10% FBS, 100 U/ml penicillin and 100  $\mu\text{g}/\text{ml}$  streptomycin. They were then kept in an incubator with 5%  $\text{CO}_2$  at 37 °C.

### 2.5. MTT assay

MTT method was used to evaluate the cytotoxicity of C, A-C-MNPs, and A-PFH/C-MNPs in AGS and 3 T3 cells. AGS and 3 T3 cells with a density of  $3 \times 10^5$  and  $2 \times 10^4$  cells/well,

respectively were cultured in 96-well microtiter plates (200  $\mu\text{L}$  per well) for 12 h in an incubator with 5%  $\text{CO}_2$  at 37  $^\circ\text{C}$ . Then, after 12 h, the cells were incubated for 24 h in the presence of C with concentrations of 5, 10, 15, and 20  $\mu\text{g}/\text{mL}$ , A-C-MNPs and A-PFH/C-MNPs with concentrations of 10, 20, 30, and 40  $\mu\text{g}/\text{mL}$  under laser irradiation (150  $\text{J}/\text{cm}^2$  fluence and 100  $\text{Mw}/\text{cm}^2$  irradiance) for 5 min at 8th h after main incubation. Next, the medium was removed by PBS, and 0.5  $\text{mg}/\text{mL}$  MTT was added in media and incubated for 4 h (50  $\text{mL}/\text{well}$ ). After incubation, the culture medium was detached and the residual crystals were liquefied in 100  $\text{mL}$  DMSO by shaking for 3 min. Finally, the optical density of the cells was assessed at  $\lambda = 570$  nm using an ELISA plate reader (RT-2100C Microplate Reader, China).

### 2.6. Apoptosis and cell cycle

Flow-cytometry was carried out to evaluate the percentage of apoptosis performed by C, A-C-MNPs and A-PFH/C-MNPs + PTT. After culturing the AGS cells according to the instructions in Section 2.5,  $3 \times 10^5$  AGS cells were cultured for 24 h per well along with the C (10  $\mu\text{g}/\text{mL}$ ), A-C-MNPs (20  $\mu\text{g}/\text{mL}$ ) and A-PFH/C-MNPs + PTT (20  $\mu\text{g}/\text{mL}$ ). Then, the AGS cells were centrifuged at 3000 rpm for 3 min at 4  $^\circ\text{C}$  and washed by cold PBS. The AGS cells were then resuspended in 100  $\text{mL}$  of Annexin V binding buffer including 0.1 M, NaCl 1.4 M,  $\text{CaCl}_2$  25 Mm, pH 7.4. Next, 2  $\mu\text{L}$  of Annexin V conjugated Alexa Fluor 488 was supplemented to the solution containing the AGS cells and kept at room temperature in the dark. Afterwards, 400  $\mu\text{L}$  of the binding buffer along with 5  $\mu\text{L}$  of 50  $\mu\text{g}/\text{mL}$  of propidium iodide were supplemented to the solution and placed in an ice box. Finally, samples were investigated by FACscan (BD Bioscience, USA).

Flow cytometry technique was used to study cell cycles. At the end of the 24 h incubation period, the AGS cells were washed with PBS and collected using trypsin and centrifugation. They were then cooled in cold ethanol (70%) and stored at  $-25$   $^\circ\text{C}$ . Afterwards, the AGS cells were dispersed again in 800  $\mu\text{L}$  of PBS. Therewith, 5  $\mu\text{L}$  of 2  $\text{mg}/\text{mL}$  RNase was added and incubated for 40 min at 37  $^\circ\text{C}$ . After incubation, the AGS cells were stained with 75  $\mu\text{L}$  of fluorescent nucleic acid dye and 1  $\text{mg}/\text{mL}$  of propidium iodide. The AGS cells were incubated at 21  $^\circ\text{C}$  for 15 min and then passed via a 40  $\mu\text{m}$  sterile filter. Finally, the AGS cells are probed by excitation at 490 nm in BD LSR II (BD Biosciences).

### 2.7. ROS assays

In order to evaluate the intracellular level of ROS in the presence of C (10  $\mu\text{g}/\text{mL}$ ), A-C-MNPs (20  $\mu\text{g}/\text{mL}$ ) and A-PFH/C-MNPs + PTT (20  $\mu\text{g}/\text{mL}$ ),  $3 \times 10^5$  AGS cells per well were cultured for 24 h. Then, 10 mM 2',7'-dichlorofluorescein was added per well and maintained up to 1 h at 37  $^\circ\text{C}$  with 5%  $\text{CO}_2$ . Next, each well was washed with PBS and homogenized carefully with 500  $\mu\text{L}$  of PBS. At the end, the fluorescent intensity was assessed using a fluorescence microplate reader (Bio-Tek Instruments, Winooski, USA).

### 2.8. Real time PCR

Isolation of total RNA was performed based on the manufacturer's protocols in control, C (10  $\mu\text{g}/\text{mL}$ ), A-C-MNPs (20  $\mu\text{g}/$

$\text{mL}$ ), and A-PFH/C-MNPs + PTT (20  $\mu\text{g}/\text{mL}$ ) groups through Trizol reagent on AGS cells. The RNA was then measured at 260–280 nm by applying a UV–VIS spectrophotometer (Eppendorf). To eliminate any contaminant genomic DNA, the RNA was treated with DNase I and cDNA was produced from 1  $\mu\text{g}$  of RNA using revert Aid First Strand cDNA Synthesis Kit (Fermentas). The following primers were used: -TNF- $\alpha$  forward 5'-CGAGTGACAAGCCTGTAGC-3', reverse 5'-GGTGTGGGTGAGGAGCACAT-3'; Bax forward 5'-TGGCAGCTGA CATGTTTTCT GAC-3' and reverse 5'-TCACCCAACC ACCCTGGTCT T-3'; Fas forward 5'-GG ACCCTCTACCTCTGGTT-3', reverse 5'-ACCTGGAGGA CAGGGCTTAT-3'; Caspase-3 forward 5'-TGGCATTGAGA CAGACA-3', reverse 5'-GGCACAAAGCGACTG-3'; GAPDH forward 5'-ACCCAGAAGACTGTGGATGG -3' and reverse 5'-TCTAGACGGCAGGTCAGGTC -3'. Quantitative PCR was executed on an ABI 7500 real-time PCR system (ABI, USA) by applying a SYBR Premix Ex Taq Reagent Kit (Takara) according to the manufacturers' recipes. The fold change in mRNA expression of TNF- $\alpha$ , Bax, Fas and Caspase-3 was calculated as  $2^{-\Delta\Delta C_t}$ .

### 2.9. Statistical analysis

Statistical analysis was carried out using SPSS software 17 (SPSS Inc., Chicago, IL, USA) version. The one-way ANOVA was performed to represent a significant range of this current work.

## 3. Results

### 3.1. Characterization of synthesized NPs

After the synthesis of MNPs by hydrothermal reaction with the introduction of an oleic acid ligand and sodium citrate as coordinating agents, their morphological properties were explained by SEM (Fig. 1B) and TEM (Fig. 1C). It was shown that A-PFH/C-MNPs are spherical in shape with an approximate size of 131.2 nm and are uniformly coated by the A with dimensions of approximately 8.3 nm. The presence of C, PFH and A increased the Zeta potential values to 27.1, 17.6,  $-9.3$  and  $-17.1$  at pH of 2.5, 5, 7.5 and 10 respectively. The potential value of  $-9.2$  in pH 7.5 indicates the stability of A-PFH/C-MNPs in physiological pH.

These images show the relatively uniform distribution of A on the NPs and the relatively narrow distribution of the A-PFH/C-MNPs. The crystalline structure of the MNPs generated was investigated applying XRD (Fig. 1D). The apparent peaks indicate lack of any additional contamination.

In this line, the outcomes of FTIR on MNPs, A, PFH, C and A-PFH/C-MNPs approved the favour loading of PFH, C and A on the MNPs (data not shown). FTIR spectra revealed that C had a peak of 3250  $\text{cm}^{-1}$ , 2950  $\text{cm}^{-1}$ , 1600  $\text{cm}^{-1}$ , 1500  $\text{cm}^{-1}$ , 1000  $\text{cm}^{-1}$ , 800  $\text{cm}^{-1}$ , and 500  $\text{cm}^{-1}$ . Also, the FTIR results show that the PFH main bonds are 1700  $\text{cm}^{-1}$ , 1600  $\text{cm}^{-1}$ , 1400  $\text{cm}^{-1}$ , and 950  $\text{cm}^{-1}$ . While, the bonds of C represented the main feature of bending and stretching vibrations in peaks on 3500–3400  $\text{cm}^{-1}$ , 1500  $\text{cm}^{-1}$ , 1250  $\text{cm}^{-1}$ , 900  $\text{cm}^{-1}$  and 500  $\text{cm}^{-1}$ . Nonetheless, when C, PFH and A were conjugated on the MNPs, the peaks

which were observed in their spectrum were modulated or disappeared.

In the following, photothermal heat generated in A-PFH/C-MNPs was explained in Fig. 2. Our outcomes illustrated that laser irradiation with 808 nm wavelength sufficiently performs the thermal activation of the A-PFH/C-MNPs.

### 3.2. C loading and PFH/C release

The output of the amount of C loaded on the MNPs based on the results of Fig. 3A shows that despite the increase in the C loading level with increasing drug concentration, the C loading efficiency decreases with increasing concentration. In this regard, the optimal C concentration for loading with efficiency higher than 60% is between 250 and 350  $\mu\text{g}/\text{mL}$  of C. Although lower C concentrations have the highest loading efficiencies, maximal utilization of nanocarrier capacity for drug delivery to AGS tissues or cancerous cells will not be observed.

In order to evaluate the reaction and response of PFH to temperature, A-PFH/C-MNPs were stored at 37, 41 and 45  $^{\circ}\text{C}$  to determine the evaporation level of PFH. As exhibited in Fig. 3B, at 37  $^{\circ}\text{C}$  similar to body temperature, the PFH release level in 60 min is very low and at the lowest level (<12%). Whereas, with increasing temperature from 37 to 41  $^{\circ}\text{C}$ , the amount of PFH release increased and after 60 min, the PFH release level reached 31%. However, at 45  $^{\circ}\text{C}$ , approximately 59% of PFH is released within 60 min. Also, the burst release of the PFH at 45  $^{\circ}\text{C}$  is faster than 41  $^{\circ}\text{C}$  and happens in 20–25 min. On the whole, the results show that higher temperatures provide stronger energy for PFH evaporation.

Likewise, the results of C release from A-PFH/C-MNPs at different pHs demonstrated that C release from A-PFH/C-MNPs according to Fig. 3C is time-dependent and pH-sensitive. In general, the C release level at pH 2.5 after 1800 min is about 73.5%, while 59.1% and 37.7% of the C were released at pH 5.0 and 7.5 after 1800 min, respectively. Thus, the results suggest that A may act as a biological gate to reduce the level of C release. Despite the rapid release of the C from the A-PFH/C-MNPs in the first 120 min, the

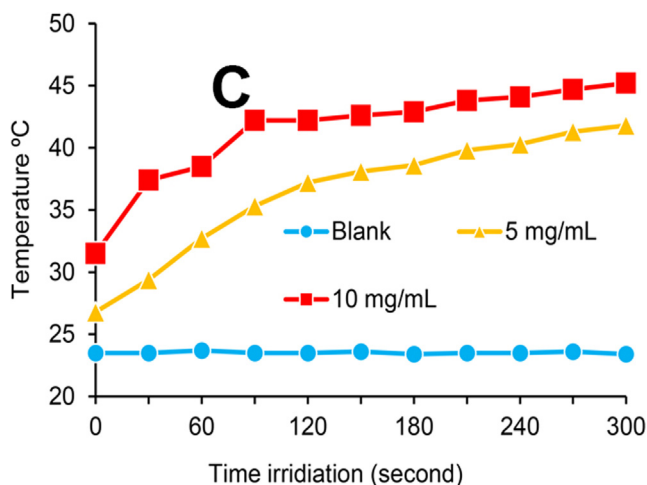


**Fig. 2** Temperature versus irradiation time with concentrations of 5 and 10 mg/mL A-PFH/C-MNPs in distilled water.

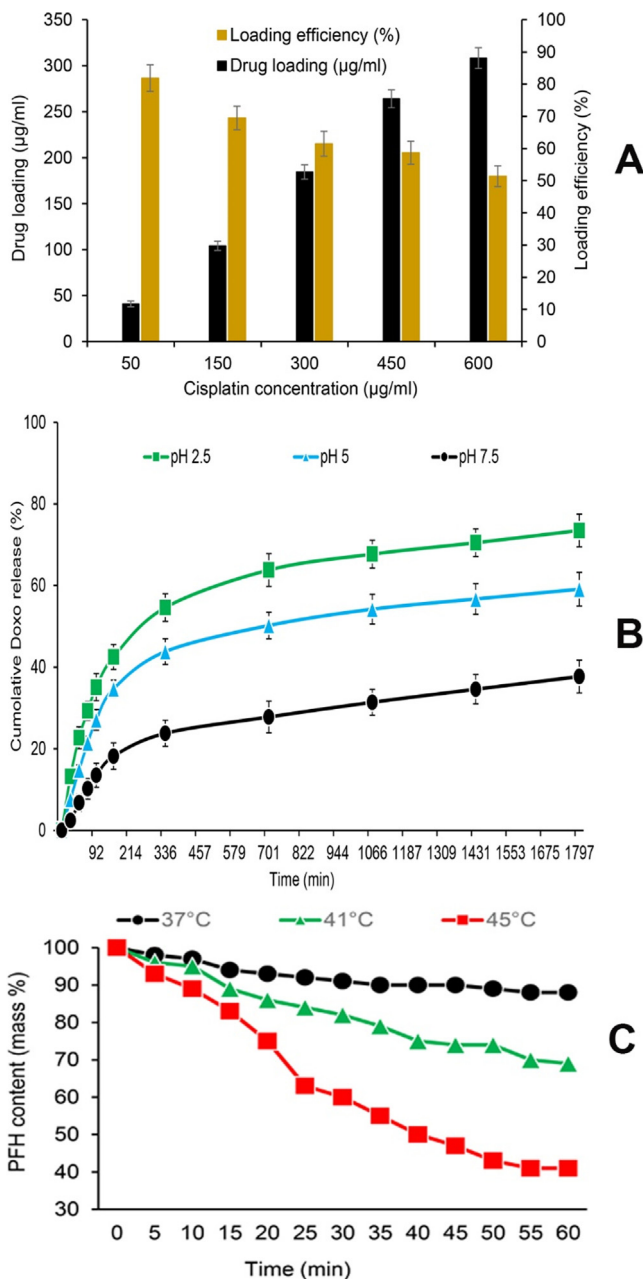


**Fig. 3** (A) Drug loading and nanocarrier efficiency, (B) quantitative analyses of cisplatin (C) release at 37  $^{\circ}\text{C}$  at different pH, (C) the perfluorohexane (PFH) content patterns monitored by thermogravimetric traces over time at 37, 41, and 45  $^{\circ}\text{C}$ .

release rate of the C is relatively constant and increasing over time. Release of more than 50–60% of the C in the first 12 h and 60–70% in 24 h of A-PFH/C-MNPs under acidic conditions has a favorable potential for C release in AGS cells.

### 3.3. Cytotoxicity assay

As mentioned earlier, the MTT technique was used to evaluate the C, A-C-MNPs and A-PFH/C-MNPs cytotoxicity on AGS cells (Fig. 4). In this study, it was found that with increasing concentrations of C and A-C-MNPs, the rate of cytotoxicity

in AGS cells increases. Whereas, the toxicity rate was much lower for 3 T3 cells with increasing C and A-C-MNPs concentrations. However, the toxicity of the free drug and nano-platform depends on the dose used (Fig. 4A). Furthermore, the results revealed that despite the higher cytotoxicity of the A-C-MNPs compared to the C at concentrations higher than 10  $\mu\text{g}/\text{mL}$ , the rate of change of both is relatively the same. Also, the toxicity results in Fig. 4B shows that the use of A-PFH/C-MNPs + PTT has the highest cytotoxicity compared to other groups. In addition, the level of toxicity increased significantly with increasing the concentration of A-PFH/C-MNPs + PTT in 3 T3 cells (Fig. 4A). Overall, the results demonstrated that increasing the concentration of A-PFH/C-MNPs combined with PTT caused the greatest cytotoxicity in AGS cells.

### 3.4. Apoptosis, cell cycle arrest and ROS production

As reported in Fig. 5A, various treatments include of C (10  $\mu\text{g}/\text{mL}$ ), A-C-MNPs (20  $\mu\text{g}/\text{mL}$ ) and A-PFH/C-MNPs + PTT (20  $\mu\text{g}/\text{mL}$ ), increase the percentage of apoptotic cells. Although the use of C increased 11.77 and 21.33 times the apoptotic cells in the late and early apoptosis compared to the control, respectively ( $**P \leq 0.01$ ), the use of A-C-MNPs exposed more induction of apoptosis in the early and late apoptosis after 24 h compared to the C ( $*P \leq 0.05$ ). The number of apoptotic cells by A-C-MNPs in early and late apoptosis increased from 25.9% to 34.8% and 19.2% to 28.7%, respectively, compared to the free drug. However, the outcomes exhibit that the synergistic effect of C and PFH via A-PFH/C-MNPs + PTT causes a significant increase in apoptotic cells in early (49.5%) and late (30.8%) apoptosis compared to A-C-MNPs. Overall, the results showed that the highest reduction in cancer cell proliferation through induction of apoptosis was in order of A-PFH/C-MNPs + PTT, A-C-MNPs and C, which could indicate the positive synergistic effects of chemotherapy and PTT.

To confirm the higher toxicity of A-C-MNPs and A-PFH/C-MNPs + PTT compared to C, ROS production was investigated. Our results in Fig. 5B depicted that the use of C and A-C-MNPs significantly increases the ROS intracellular level

up to 209 ( $**P < 0.01$ ) and 278 ( $**P < 0.01$ ) units, respectively, compared to the control group. However, the use of A-PFH/C-MNPs + PTT produced the highest ROS up to 3.06 folds (with 389 units) of the control group, 1.86 times the C group and 1.39 folds of the A-C-MNPs group. Therefore, it was found that A-PFH/C-MNPs + PTT and A-C-MNPs could inhibit the proliferation of AGS cancerous cell by generation of ROS.

Also, as illustrated in Fig. 5C, C significantly increased the AGS cell population in the subG1 phase by 1.64 times compared to the control group ( $**P < 0.01$ ). Likewise, A-C-MNPs caused a significant increase in AGS cell population in the subG1 phase compared to the control group. In addition, the use of nanocarriers has significantly increased the concentration of AGS cells in the subG1 phase compared to the free drug ( $*P < 0.05$ ). While the highest AGS cell population observed in the subG1 phase was related to A-PFH/C-MNPs + PTT, which was 3.06 folds higher than the control group ( $***P < 0.001$ ). On the other hand, the highest AGS cell concentration in phase S was related to A-PFH/C-MNPs + PTT, A-C-MNPs and C, which indicates an effective increase in the combination of chemotherapy and PPT.

### 3.5. Cell death mechanisms

The results of the toxicity mechanism based on Fig. 6 show that significant changes in the expression of TNF- $\alpha$ , Fas, Bax, and Caspase-3 genes were observed in the presence of nanocarriers and drugs. For example, the use of C significantly increased the expression of TNF- $\alpha$ , Fas, Bax, and Caspase-3 genes compared to the control group. But, the use of A-C-MNPs displayed a significant increase in TNF- $\alpha$ , Bax, and Caspase-3 genes compared to free drugs, whereas it did not induce a significant regulation in the expression of Fas gene compared to C group. On the other hand, the inhibitory effects on AGS cancerous cells by increasing the expression of TNF- $\alpha$ , Bax, and Caspase-3 genes in combination therapy by chemotherapy and PTT based on A-PFH/C-MNPs resulted in a significant difference compared to the A-C-MNPs and free drug groups. However, A-PFH/C-MNPs + PTT did not show a significant upregulation in the Fas gene compared to the C

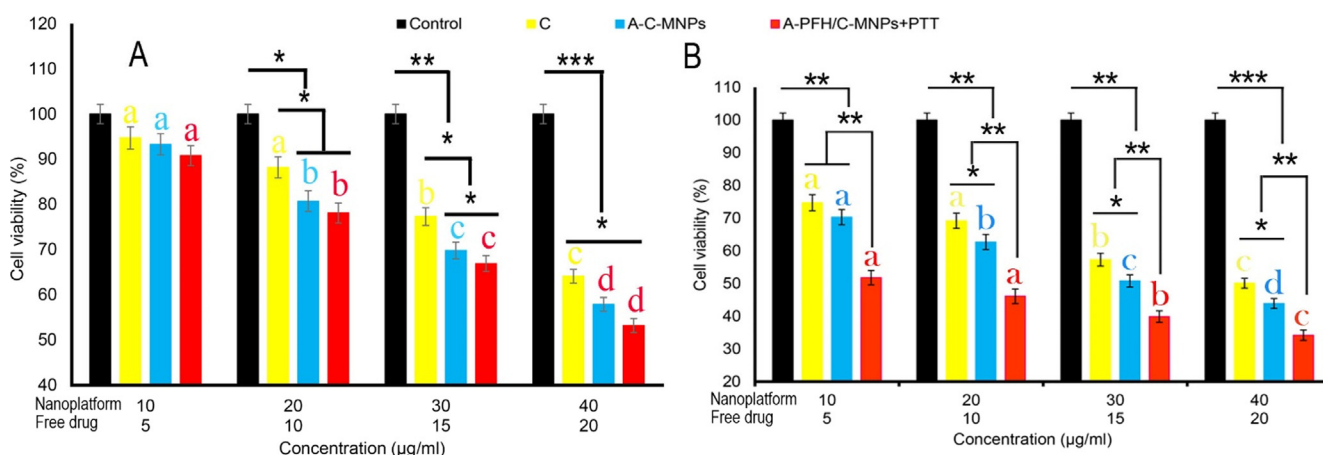


**Fig. 4** Cytotoxicity assay of cisplatin (C), albumin-cisplatin-magnetite nanoparticle (A-C-MNPs), and albumin-perfluorohexane/cisplatin-MNPs plus PTT (A-PFH/C-MNPs + PTT) in 3 T3 cells (A) and AGS (B) cells.  $*P < 0.05$ ,  $**P < 0.01$  and  $***P < 0.001$  for a difference of treatment groups. <sup>a,b,c,d</sup>Least square means with different letters in superscripts are different at  $*P < 0.05$ .

and A-C-MNPs. In fact, the most induced TNF- $\alpha$  and Bax pathways of apoptosis are related to A-PFH/C-MNPs + PTT and A-C-MNPs, and the induction of the Fas pathway

is related to C and A-C-MNPs. Taken together, these results indicate that the greatest increase in Caspase-3 through intrinsic and extrinsic apoptotic pathways in AGS cancerous cells is mediated by A-PFH/C-MNPs + PTT, followed by A-C-MNPs and C.

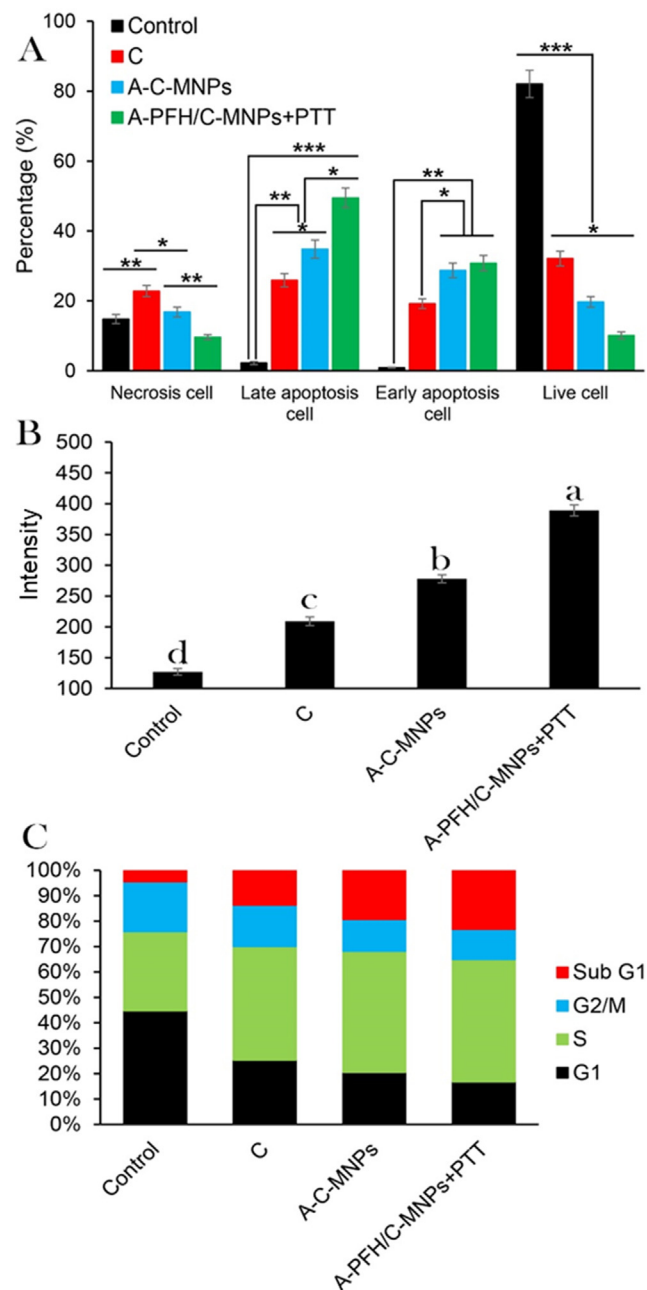


**Fig. 5** (A) Quantification of cell necrosis and apoptosis measured using propidium iodide (PI) and Annexin V-FITC staining in AGS cancerous cells determined by flow cytometry assay. Control, cisplatin (C), albumin-cisplatin-magnetite nanoparticle (A-C-MNPs), and albumin-perfluorohexane/cisplatin-MNPs plus PTT (A-PFH/C-MNPs + PTT), (B) the effects of C, A-C-MNPs and A-PFH/C-MNPs + PTT on the ROS production, and (C) flow cytometry-based assay of the cell cycle: control, cisplatin, A-C-MNPs and A-PFH/C-MNPs + PTT. \* $P < 0.05$ , \*\* $P < 0.01$  and \*\*\* $P < 0.001$  for a difference of treatment groups. <sup>a,b,c,d</sup>Least square means with different letters in superscripts are different at \* $P < 0.05$ .

#### 4. Discussion

Because protein-coated MNPs have very low cytotoxicity and high stability in bioactivity, they are very important in drug delivery, imaging, PTT, magnetic fields, and combination therapies with the integration of the above methods. Here, after synthesizing A-PFH/C-MNPs by hydrothermal method and examining physicochemical properties by SEM (Fig. 1B), TEM (Fig. 1C), and XRD (Fig. 1D) techniques, we showed that the uniform distribution of NPs was in accordance with the findings of Gokduman (2019) and Sharifi et al. (2020b). Whereas, synthesis of MNPs with relatively narrow and uniform range and relatively high surface area is a main challenge (Ali et al. 2016, Sharifi et al. 2020c). Also, similar to the studies of Gokduman (2019), Hormozi and Esmaceli (2019) and Teng et al. (2017), the results of this study indicate a uniform loading of A on MNPs and high loading of C and PFH. Although the porosity of the synthesized MNPs was not investigated in this study, in comparison with the result of Gokduman (2019) the MNPs synthesized in this study have the highest drug loading percentage up to 61% (Fig. 3A).

As shown in Fig. 3B, the drug release rate in A-PFH/C-MNPs depends on the environment acidity, and optimally the burst release time and drug release percentage in these nanocarriers improve with changes in environmental acidity. The results of drug release in this study in line with the results of Abedi et al. (2019) and Chen et al. (2019) indicate the high sensitivity of nanocarriers produced to environmental pH. Overall, the results indicated that by changing the neutral to acidic conditions, the rate of drug release increases, which is potentially very suitable for targeting the drug in AGS cancerous cells due to the acidity of their environment. As well, the results of this report are similar to the findings of Su et al. (2015) and Guo et al. (2018) illustrated that MNPs, like other metal oxide NPs, have a high release potential for the PFH based on the thermal responses of the nanocarriers.

The cytotoxic effects of A-PFH/C-MNPs and free drugs on gastric cancer cells indicate that cell growth inhibition is strongly dependent on C dose and MNPs (Fig. 4). This report is consistent with the outputs of Gokduman (2019) and Mandriota et al. (2019) who demonstrated that the use of nanocarriers in drug delivery increases intracellular cytotoxicity due to drug dose changes. On the other hand, this study, similar to the results of Sharifi et al. (2020a) and Su et al. (2015) revealed that the combination of chemotherapy and PTT in cancerous cells further improves the anticancer effects of developed nano system. The degree of cytotoxicity of MNPs containing anticancer drugs is generally expressed by their catalytic effects through ROS production (Sharifi et al. 2020c, Canaparo et al. 2021), DNA damage (Revia and Zhang 2016), and mitochondrial dysfunction (Khan et al. 2012). In this regard, the results of this study in accordance with the findings of Velavan et al. (2018) and Baneshi et al. (2019) showed that the use of protein-coated MNPs containing drug in comparison with free drug increases the induction of

apoptosis by increasing the generation of intracellular ROS. Likewise, the results of the cell cycle indicate the accumulation of AGS cancerous cells in subG1 phase, which in accordance with previous findings that nanoplateforms are able to stop the proliferation of cancerous cells (Zhang et al. (2015) Lu et al. (2018)). The higher anticancer effects of combination therapy in this study are similar to the findings of Su et al. (2015) and Guo et al. (2018), which could indicate the induction of a synergistic anticancer effect enabled by developed platform. Therefore, inhibiting the proliferation of AGS cancerous cells based on the combination therapy can play a promising role in anticancer activity of developed platforms. Conversion of light into heat involves two physical processes, electron–electron and electron–phonon in femtoseconds and picoseconds, respectively, which quickly convert the absorbed light into heat. Due to the small size of the NPs, almost 100% of the

emitted light is converted into thermal energy (Bohren and Huffman 1998). Therefore, when the cells are irradiated, the cancer cells are sensitive to the temperature-dependent cell death.

Although the positive effects of A-PFH/C-MNPs on the cell cycle arrest and their inhibitory effects via apoptosis are evident in Fig. 5, the use of PTT can induce more severe inhibitory effects on AGS cancer cell growth relative to the cells treated only with A-C-MNPs. In this regard, the outputs of the cytotoxicity mechanism in Fig. 6 confirm that the combination of chemotherapy and PTT increased the expression of genes in the extrinsic (TNF- $\alpha$  gene) and intrinsic (Bax gene) pathways of apoptosis. Our findings were similar to the results of Li et al. (2019) who revealed that the simultaneous use of chemotherapy and PTT enabled by metal oxide NPs induces apoptosis via expression of TNF- $\alpha$  (extrinsic apoptosis

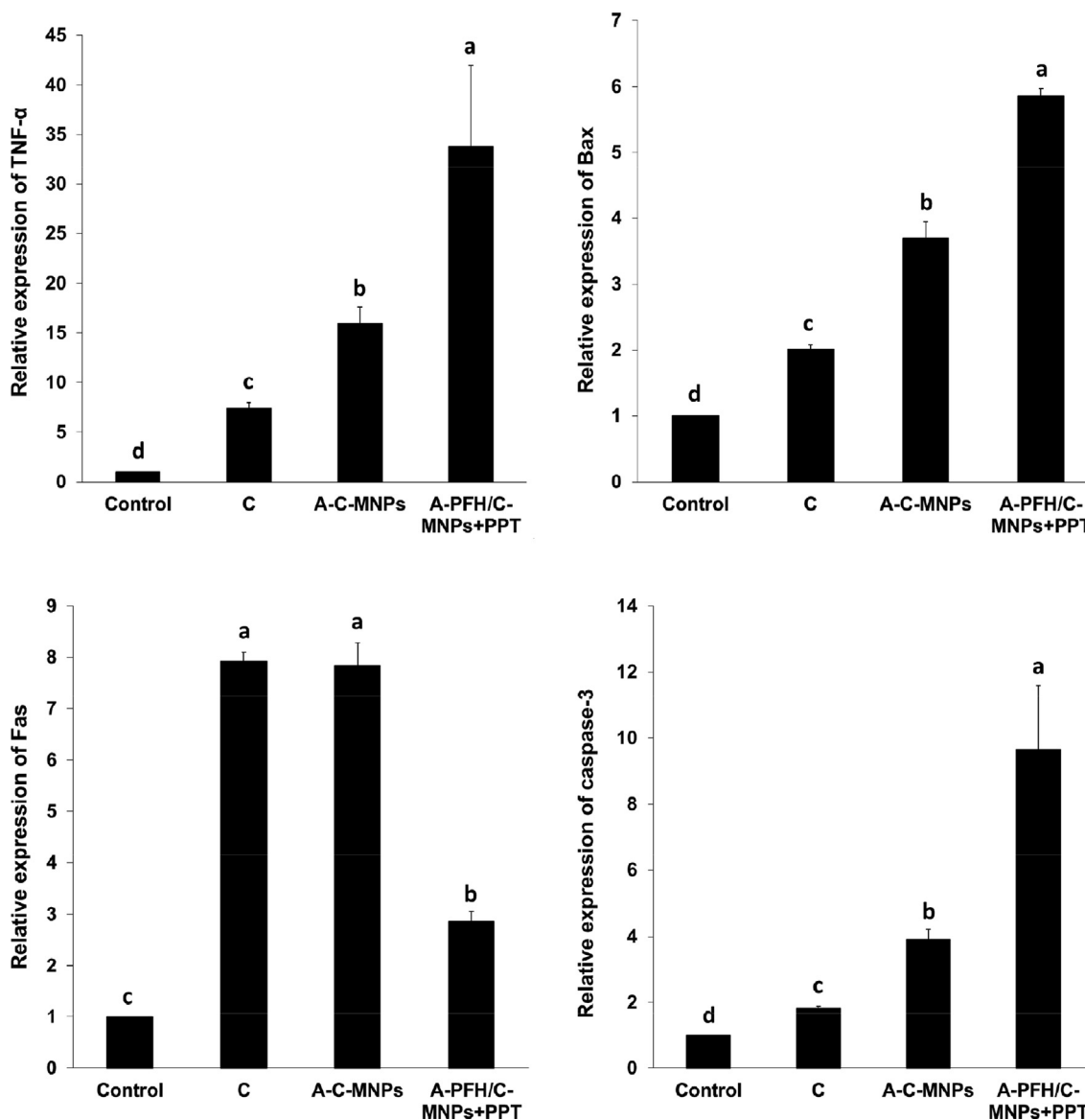


**Fig. 6** Effect of the control, cisplatin, albumin-cisplatin-magnetite nanoparticle (A-C-MNPs), and albumin-perfluorohexane/cisplatin-MNPs plus PTT (A-PFH/C-MNPs + PTT) on the expression of TNF- $\alpha$ , Bax, Fas and Caspase-3 mRNA, in the AGS cancerous cells. <sup>a,b,c,d</sup>Least square means with different letters in superscripts are different at \*P < 0.05.

pathway initiator) and Bax (intrinsic apoptosis pathway initiator) genes. In addition, the results of this study, similar to the findings of Lu et al. (2018), showed that the combination of chemotherapy and PTT can induce the activation of Caspase-3 signalling pathway.

## 5. Conclusions

In general, our results indicate the synthesis of A-PFH/C-MNPs with a spherical shape, relatively narrow distribution and drug loading capacity of over 60%. Also, the C and PFH release profile showed that the synthesized NPs are not only sensitive to the environmental pH, but also have a favourable thermal response in PTT. In addition, A-PFH/C-MNPs + PTT enhanced anticancer activity by increasing intracellular ROS, inducing apoptosis and increasing the population of AGS cancerous cells in the subG1 phase. Based on the findings, it can be said that MNPs can be considered as a suitable platform for combination of therapeutics in the treatment of gastric cancer.

## Declaration of Competing Interest

The authors declare that they have no known competing financial interests or personal relationships that could have appeared to influence the work reported in this paper.

## References

- Abedi, M., Abolmaali, S.S., Abedanzadeh, M., Borandeh, S., Samani, S.M., Tamaddon, A.M., 2019. Citric acid functionalized silane coupling versus post-grafting strategy for dual pH and saline responsive delivery of cisplatin by Fe<sub>3</sub>O<sub>4</sub>/carboxyl functionalized mesoporous SiO<sub>2</sub> hybrid nanoparticles: a-synthesis, physicochemical and biological characterization. *Mater. Sci. Eng. C* 104, 109922.
- Agnihotri, S., Mohan, T., Jha, D., Gautam, H.K., Roy, I., 2020. Dual modality FeS nanoparticles with reactive oxygen species-induced and photothermal toxicity toward pathogenic bacteria. *ACS Omega* 5, 597–602.
- Ali, A., Hira Zafar, M.Z., ul Haq, I., Phull, A.R., Ali, J.S., Hussain, A., 2016. Synthesis, characterization, applications, and challenges of iron oxide nanoparticles. *Nanotechnology, science and applications*. 9, 49
- Baneshi, M., Dadfarnia, S., Shabani, A.M.H., Sabbagh, S.K., Haghgoo, S., Bardania, H., 2019. A novel theranostic system of AS1411 aptamer-functionalized albumin nanoparticles loaded on iron oxide and gold nanoparticles for doxorubicin delivery. *Int. J. Pharm.* 564, 145–152.
- Batooei, S., Khajeali, A., Khodadadi, R., Islamian, J.P., 2020. Metal-based nanoparticles as radio-sensitizer in gastric cancer therapy. *J. Drug Delivery Sci. Technol.* 56, 101576.
- Bejjanki, N.K., Xu, H., Xie, M., 2021. GSH triggered intracellular aggregated-cisplatin-loaded iron oxide nanoparticles for overcoming cisplatin resistance in nasopharyngeal carcinoma. *Journal of Biomaterials Applications*. 36, 0885328220982151.
- Bohren, C., Huffman, D. 1998. Absorption and scattering of light by small particles: Wiley Science. Weinheim, Germany.
- Canaparo, R., Foglietta, F., Limongi, T., Serpe, L., 2021. Biomedical applications of reactive oxygen species generation by metal nanoparticles. *Materials* 14, 53.
- Chen, D., Lin, X., Gao, J., Shen, L., Li, Z., Dong, B., Zhang, C., Zhang, X., 2018. Weel1 inhibitor AZD1775 combined with cisplatin potentiates anticancer activity against gastric cancer by increasing DNA damage and cell apoptosis. *BioMed Research International*. 2018.
- Chen, J., Liu, J., Hu, Y., Tian, Z., Zhu, Y., 2019. Metal-organic framework-coated magnetite nanoparticles for synergistic magnetic hyperthermia and chemotherapy with pH-triggered drug release. *Sci. Technol. Adv. Mater.* 20, 1043–1054.
- Chen, F., Qin, X., Xu, G., Gou, S., Jin, X., 2017. Reversal of cisplatin resistance in human gastric cancer cells by a wogonin-conjugated Pt (IV) prodrug via attenuating Casein Kinase 2-mediated Nuclear Factor- $\kappa$ B pathways. *Biochem. Pharmacol.* 135, 50–68.
- Chen, W., Yang, Z., 2020. Human gastric carcinoma cells targeting peptide-functionalized iron oxide nanoparticles delivery for magnetic resonance imaging. *Process Biochem.* 99, 171–178.
- Ghosh, S., 2019. Cisplatin: the first metal based anticancer drug. *Bioorg. Chem.* 88, 102925.
- Gokduman, K., 2019. Sensitization of cisplatin-resistant ovarian cancer cells by magnetite iron oxide nanoparticles: an in vitro study. *Nanomedicine* 14, 3177–3191.
- Guo, Y., Wang, X.-Y., Chen, Y.-L., Liu, F.-Q., Tan, M.-X., Ao, M., Yu, J.-H., Ran, H.-T., Wang, Z.-X., 2018. A light-controllable specific drug delivery nanoplatform for targeted bimodal imaging-guided photothermal/chemo synergistic cancer therapy. *Acta Biomater.* 80, 308–326.
- Hormozi, N., Esmaeili, A., 2019. Synthesis and correction of albumin magnetic nanoparticles with organic compounds for absorbing and releasing doxorubicin hydrochloride. *Colloids Surf. B Biointerfaces* 182, 110368.
- Jiang, D., Ni, D., Rosenkrans, Z.T., Huang, P., Yan, X., Cai, W., 2019. Nanozyme: new horizons for responsive biomedical applications. *Chem. Soc. Rev.* 48, 3683–3704.
- Khan, M.I., Mohammad, A., Patil, G., Naqvi, S., Chauhan, L., Ahmad, I., 2012. Induction of ROS, mitochondrial damage and autophagy in lung epithelial cancer cells by iron oxide nanoparticles. *Biomaterials* 33, 1477–1488.
- Khan, M.A., Singh, D., Ahmad, A., Siddique, H.R., 2021. Revisiting inorganic nanoparticles as promising therapeutic agents: a paradigm shift in oncological theranostics. *Eur. J. Pharm. Sci.* 164, 105892.
- Li, W., Xue, B., Shi, K., Qu, Y., Chu, B., Qian, Z., 2019. Magnetic iron oxide nanoparticles/10-hydroxy camptothecin co-loaded nanogel for enhanced photothermal-chemo therapy. *Appl. Mater. Today* 14, 84–95.
- Liang, X., Zhu, J., Li, Y., Xu, Y., Chen, K., Lv, L., Mao, W., 2020. Treatment strategies for metastatic gastric cancer: chemotherapy, palliative surgery or radiotherapy? *Future Oncol.* 16, 91–102.
- Lin, X.-M., Li, S., Zhou, C., Li, R.-Z., Wang, H., Luo, W., Huang, Y.-S., Chen, L.-K., Cai, J.-L., Wang, T.-X., 2019. Cisplatin induces chemoresistance through the PTGS2-mediated anti-apoptosis in gastric cancer. *Int. J. Biochem. Cell Biol.* 116, 105610.
- Lu, Q., Dai, X., Zhang, P., Tan, X., Zhong, Y., Yao, C., Song, M., Song, G., Zhang, Z., Peng, G., Guo, Z., Ge, Y., Zhang, K., Li, Y., 2018. Fe<sub>3</sub>O<sub>4</sub>@Au composite magnetic nanoparticles modified with cetuximab for targeted magneto-photothermal therapy of glioma cells. *Int. J. Nanomed.* 13, 2491–2505.
- Mandriota, G., Di Corato, R., Benedetti, M., De Castro, F., Fanizzi, F.P., Rinaldi, R., 2019. Design and application of cisplatin-loaded magnetic nanoparticle clusters for smart chemotherapy. *ACS Appl. Mater. Interfaces* 11, 1864–1875.
- Manohar, S., Leung, N., 2018. Cisplatin nephrotoxicity: a review of the literature. *J. Nephrol.* 31, 15–25.
- Marin, J.J., Perez-Silva, L., Macias, R.I., Asensio, M., Peleteiro-Vigil, A., Sanchez-Martin, A., Cives-Losada, C., Sanchon-Sanchez, P., Sanchez De Blas, B., Herraez, E., 2020. Molecular bases of mechanisms accounting for drug resistance in gastric adenocarcinoma. *Cancers* 12, 2116.
- Maximenko, A., Depciuch, J., Łopuszyńska, N., Stec, M., Świątkowska-Warkocka, Ż., Bayev, V., Zieliński, P.M., Baran, J., Fedotova, J., Węglarz, W.P., 2020. Fe<sub>3</sub>O<sub>4</sub>@SiO<sub>2</sub>@Au nanoparticles for MRI-guided chemo/NIR photothermal therapy of cancer cells. *RSC Adv.* 10, 26508–26520.
- Nagaraju, G.P., Srivani, G., Dariya, B., Chalikonda, G., Farran, B., Behera, S.K., Alam, A., Kamal, M.A., 2021. Nanoparticles guided

- drug delivery and imaging in gastric cancer. *Semin. Cancer Biol.* 69, 69–76.
- Norouzi, M., Yathindranath, V., Thliveris, J.A., Kopec, B.M., Siahaan, T.J., Miller, D.W., 2020. Doxorubicin-loaded iron oxide nanoparticles for glioblastoma therapy: a combinational approach for enhanced delivery of nanoparticles. *Sci. Rep.* 10, 11292.
- Prestayko, A.W., 2013. *Cisplatin: current status and new developments*. Academic Press.
- Revia, R.A., Zhang, M., 2016. Magnetite nanoparticles for cancer diagnosis, treatment, and treatment monitoring: recent advances. *Mater. Today* 19, 157–168.
- Sharifi, M., Hasan, A., Nanakali, N.M.Q., Salihi, A., Qadir, F.A., Muhammad, H.A., Shekha, M.S., Aziz, F.M., Amen, K.M., Najafi, F., Yousefi-Manesh, H., Falahati, M., 2020a. Combined chemo-magnetic field-photothermal breast cancer therapy based on porous magnetite nanospheres. *Sci. Rep.* 10, 5925.
- Sharifi, M., Jafari, S., Hasan, A., Paray, B.A., Gong, G., Zheng, Y., Falahati, M., 2020b. Antimetastatic activity of lactoferrin-coated mesoporous maghemite nanoparticles in breast cancer enabled by combination therapy. *ACS Biomater. Sci. Eng.* 6, 3574–3584.
- Sharifi, M., Rezayat, S.M., Akhtari, K., Hasan, A., Falahati, M., 2020c. Fabrication and evaluation of anti-cancer efficacy of lactoferrin-coated maghemite and magnetite nanoparticles. *J. Biomol. Struct. Dyn.* 38, 2945–2954.
- Shimura, T., Dayde, D., Wang, H., Okuda, Y., Iwasaki, H., Ebi, M., Kitagawa, M., Yamada, T., Yamada, T., Hanash, S.M., 2020. Novel urinary protein biomarker panel for early diagnosis of gastric cancer. *Br. J. Cancer* 123, 1656–1664.
- Song, S., Du, L., Jiang, H., Zhu, X., Li, J., Xu, J., 2016. Paris Saponin I Sensitizes Gastric Cancer Cell Lines to Cisplatin via Cell Cycle Arrest and Apoptosis. *Medical science monitor : international medical journal of experimental and clinical research.* 22, 3798–3803
- Su, Y.-L., Fang, J.-H., Liao, C.-Y., Lin, C.-T., Li, Y.-T., Hu, S.-H., 2015. Targeted mesoporous iron oxide nanoparticles-encapsulated perfluorohexane and a hydrophobic drug for deep tumor penetration and therapy. *Theranostics* 5, 1233–1248.
- Teng, Z., Wang, R., Zhou, Y., Kolios, M., Wang, Y., Zhang, N., Wang, Z., Zheng, Y., Lu, G., 2017. A magnetic droplet vaporization approach using perfluorohexane-encapsulated magnetic mesoporous particles for ultrasound imaging and tumor ablation. *Biomaterials* 134, 43–50.
- Thrift, A.P., El-Serag, H.B., 2020. Burden of gastric cancer. *Clin. Gastroenterol. Hepatol.* 18, 534–542.
- Velavan, B., Divya, T., Sureshkumar, A., Sudhandiran, G., 2018. Nano-chemotherapeutic efficacy of (–)-epigallocatechin 3-gallate mediating apoptosis in A549 cells: Involvement of reactive oxygen species mediated Nrf2/Keap1 signaling. *Biochem. Biophys. Res. Commun.* 503, 1723–1731.
- Wang, H.-Y., Hou, L., Li, H.-L., Wang, X., Cao, Y., Zhang, B.-Y., Wang, J.-T., Wei, S.-J., Dang, H.-W., Ran, H.-T., 2020. A nanosystem loaded with perfluorohexane and rose bengal coupled upconversion nanoparticles for multimodal imaging and synergetic chemo-photodynamic therapy of cancer. *Biomater. Sci.* 8, 2488–2506.
- Xiao, Y., Gao, Y., Li, F., Deng, Z., 2020. Combinational dual drug delivery system to enhance the care and treatment of gastric cancer patients. *Drug Deliv.* 27, 1491–1500.
- Xu, L., Qiu, X., Zhang, Y., Cao, K., Zhao, X., Wu, J., Hu, Y., Guo, H., 2016. Liposome encapsulated perfluorohexane enhances radiotherapy in mice without additional oxygen supply. *J. Transl. Med.* 14, 1–9.
- Yu, D., Gu, J., Chen, Y., Kang, W., Wang, X., Wu, H., 2020. Current strategies to combat Cisplatin-induced ototoxicity. *Front. Pharmacol.* 11, 999.
- Yu, M., Xu, X., Cai, Y., Zou, L., Shuai, X., 2018. Perfluorohexane-cored nanodroplets for stimulations-responsive ultrasonography and O<sub>2</sub>-potentiated photodynamic therapy. *Biomaterials* 175, 61–71.
- Zhang, W., Qiao, L., Wang, X., Senthilkumar, R., Wang, F., Chen, B., 2015. Inducing cell cycle arrest and apoptosis by dimercaptosuccinic acid modified Fe<sub>3</sub>O<sub>4</sub> magnetic nanoparticles combined with nontoxic concentration of bortezomib and gambogic acid in RPMI-8226 cells. *Int. J. Nanomed.* 10, 3275–3289.
- Zhou, D., Li, C., He, M., Ma, M., Li, P., Gong, Y., Ran, H., Wang, Z., Wang, Z., Zheng, Y., 2016. Folate-targeted perfluorohexane nanoparticles carrying bismuth sulfide for use in US/CT dual-mode imaging and synergistic high-intensity focused ultrasound ablation of cervical cancer. *J. Mater. Chem. B* 4, 4164–4181.